



Smoothed Particle Hydrodynamics Method for Three-Dimensional Open Channel Flow Simulations

D. López^{1†}, T. Ramos¹, P. Sánchez², R. Marivela³, R. Díaz¹, J. J. Rebollo¹, F. R. Andrés¹,
 V. Cuellar⁴, M. De Blas⁵ and J. L. García⁶

¹ *Hydraulics Laboratory, Centro de Estudios Hidrográficos, Madrid, Spain*

² *Hydraulic Engineering Master Student at TU Delft, Delft, The Netherlands*

³ *Virginia Tech, Blacksburg, Virginia, USA*

⁴ *Wawecrafters. SA., Madrid, Spain*

⁵ *Conhidra, Madrid, Spain*

⁶ *Polytechnic University of Madrid, Madrid, Spain*

† *Corresponding Author Email: david.lopez@cedex.es*

(Received November 20, 2017; accepted July 3, 2018)

ABSTRACT

To date, the Smoothed Particle Hydrodynamics (SPH) method has been successfully applied to reproduce the hydrodynamics behind three-dimensional flow-structure interactions. However, as soon as the effect of flow resistance becomes significant, the results obtained are not consistent with observations. This is the case for open channel flows (OCF), in which the water surface is largely influenced by the boundary friction. The roughness generated by the current boundary condition methodologies is solely numerical and cannot be associated to physical values of friction. In light of this challenge, the authors present a novel formulation for the friction boundary condition. The new implementation includes an additional shear stress at the boundaries to reproduce roughness effects, allowing for the adequate three-dimensional simulation of open channel flows using the SPH method. Finally, in order to reduce the high computational cost, typical of the Lagrangian models, without interfering in the representativeness of the SPH simulations, a criterion to define the adequate fluid particle size is proposed.

Keywords: Smoothed Particle Hydrodynamics (SPH); Open Channel Flow (OCF); Three-dimensional Simulations; Bed roughness; Boundary friction methodology; Computational Fluid Dynamics (CFD).

NOMENCLATURE

a, b	velocity profile coefficients	H	water depth
a_f	acceleration exerted by the boundary particles	k	von karman's constant
A	subscript indicating reference particle	k_s	nikuradse's roughness coefficient
B	subscript indicating neighbor particle	n	mannings coefficient
c_s	speed of sound at the reference density	m	particle mass
C_e	effective distance to contour coefficient	p_1, p_2	exponents of the repulsive force
C_f	friction coefficient	p_i	pressure of particle i
C_{rough}	roughness coefficient	q	discharge rate per unit width
C_a	viscous coefficient	r	distance between fluid and boundary particles
D_a	dimensionless discretization number	R_h	hydraulic radius
d_0	repulsive force constant	r_0	lennard Jones forces radius
d_e	effective distance from contour to friction force	S_o	channel bed slope
d_x	interparticle distance between fluid particles	S_w	water surface slope
d_{sc}	boundary interparticle distance	V	mean velocity in channel cross section
$f(r)$	repulsive force of a boundary particle	v	velocity vector
g	gravitational acceleration	v^*	shear velocity
		v_{part}	fluid particle velocity
		W	kernel function

α	artificial viscosity coefficient	ρ_0	reference density
β	monaghan viscous force parameter	ρ_i	particle density
γ	polytropic index for the equation of state	τ_b	bottom shear stress
ν_t	turbulent kinematic viscosity		

1. INTRODUCTION

The Smoothed Particle Hydrodynamics (SPH) method is a Lagrangian gridless approach introduced by Lucy (1977) and Gingold and Monaghan (1977) in the late seventies. Although initially developed for compressible fluids, the method was adapted and adjusted to address hydrodynamic problems (Monaghan (1994)). The reformulation of the method provided the Computational Fluid Dynamics (CFD) community with a new technique to describe the movement of the fluids without the Eulerian models restrictions (Lui and Liu (2003)).

So far, many authors such as Gatti *et al.* (2007) and López *et al.* (2009) have successfully applied this methodology to account for hydrodynamic phenomena in their simulations, obtaining excellent outcomes when reproducing three-dimensional flow-structure interactions. However, as soon as the water surface starts being influenced by the boundary resistance, the results obtained are at odds with reality. This is the case when the SPH method is applied to simulate large open channel flow areas (Nezu and Rodi (1986)). According to López *et al.* (2011), the existing boundary techniques are not entirely capable of defining the water surface elevation because they do not correctly recreate three dimensional boundary roughness effects. Therefore, implementing a boundary condition that is able to reproduce the effects of flow resistance is essential for further development and use of the SPH method to simulate three-dimensional OCF scenarios.

This problem was seen by Gómez-Gesteira *et al.* (2010) and López *et al.* (2011), who increased the boundary roughness by placing boundary particles outside the theoretical edge. Even though these extra boundary particles seemed to hinder the flow of fluid particles next to the boundary, they also introduced high disturbances into the flow, leading to inaccurate results. Chen *et al.* (2015) and Kazemi *et al.* (2017) also came out with innovative procedures, implementing friction in SPH for shallow water equations. Despite all the efforts, the problem remains poorly defined when, instead of adopting a depth-integrated approach, the Navier-Stokes equations are solved in the $x - z$ plane.

The appearance of supercomputing techniques based on parallel Message Passing Interface (MPI) paradigm (Grassa (2007)) or Compute Unified Device Architecture (CUDA) (Héroult *et al.* (2010), Crespo *et al.* (2011)) has enhanced the applicability of the method by increasing the simulation extents and reducing the computation time steps. However, a large number of particles is still required in order to accurately simulate river reaches in three dimensions. This is why, in addition to the lack of an accurate method that implements friction boundary conditions in three-dimensional

simulations, the high computational cost stands as the second major constrain for the use of the SPH method to reproduce OCF. In order to reduce the computational load, the continuum must be discretized with the maximum possible fluid particle size without affecting results representativity. With the purpose of finding such optimum dimensions, a similarity criterion is needed. While Froude's similarity law is used in physical model tests for designing OCF experiments, in numerical simulations, a proper criterion that guarantees hydraulic similarity has not been yet formulated.

This paper introduces a novel proposal called Boundary Friction Force Method. The new methodology implements an additional shear stress at the boundaries to reproduce roughness friction in three dimensional OCF simulations. The reader should note that the use of this procedure requires a proper interpretation of the shear stress formulation commonly used for turbulent flows. The concepts, shear velocity and average velocity, handled in Eulerian models, cannot be transposed to Lagrangian models in which particles carry the fluid properties. Thus, instead of defining shear stress with the depth-averaged velocity V , the velocity of the fluid particle that interacts with the boundary is introduced, v_{part} . Furthermore, the dimensionless friction coefficient C_f , which depends on the Reynolds number and the relative roughness, is substituted by a roughness coefficient C_{rough} . The suggested coefficient allows fitting the friction condition to a desired Manning's n or Nikuradse's k_s roughness value, while preserving the hydraulic similarity of the new formulation.

In this investigation, the proposed methodology has been analyzed and calibrated by means of a very simple case study composed of a rectangular-shaped straight channel with uniform steady flow. The simulations have been performed using the SPHERIMENTAL software developed by López and Cuellar (2011). By adopting the Lennard-Jones boundary technique and Monaghan's artificial viscosity turbulence method (Monaghan and Gingold (1983)), the analysis of the new formulation frictional effects and the influence of its characteristic parameters has been conducted. This work also gives a general formulation of the velocity and turbulent viscosity profiles as a function of two dimensionless parameters: the relative particle size, D_a , and the artificial viscosity coefficient, α . Finally, a hydraulic similarity criterion has been proposed to assure representativeness of SPH simulations in open channel flow.

The paper starts with a brief introduction to the main principles of the SPH method, including some details regarding the Lennard-Jones boundary condition as well as the SPHERIMENTAL software used in this research. Then, the conceptual

framework and the implementation of the Boundary Force Method are explained with an inclusive overview of the new formulation. This is followed by a description of the case study. Finally, the main findings concerning the frictional effects of the new boundary friction method and the similarity criterion are discussed.

2. SPH NUMERICAL MODELING FORMULATION

2.1 Numerical Method

The SPH method is a Lagrangian particle approach in which the basic idea is to discretize the continuum by means of a finite number of particles. Due to the constant interaction between these particles, field values for physical variables such as pressure, density, velocity, vorticity, temperature, and position, can be obtained from discrete values of neighboring fluid particles using an averaging scheme, the so-called kernel function. To put it another way, the motion of the fluid can be perfectly described by the motion of the particles. Figure 1 sketches an example of interpolation kernel, being A the target particle and B the neighbor particles.

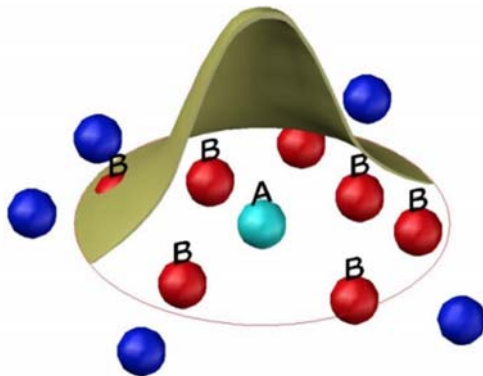


Fig. 1. SPH interpolation kernel sketch.

The Lagrangian form of the Navier-Stokes equations for a weakly compressible viscous fluid are transformed into a system of ordinary differential equations that are written as:

$$\frac{d\rho_A}{dt} = \sum_B m_B (v_A - v_B) \cdot \nabla W_{AB} \quad (1)$$

$$\frac{dv_A}{dt} = -\sum_B m_B \left(\frac{p_B}{\rho_B^2} + \frac{p_A}{\rho_A^2} + \Pi_{AB} \right) \cdot \nabla_A W_{AB} + g \quad (2)$$

where m is the particle mass, ρ the density, v the velocity, p the pressure, g the gravitational acceleration, and t the time. Finally, ∇W_{AB} expresses the gradient of the SPH kernel function between A and B. The additional term Π_{AB} from Eq. (2) symbolizes the viscous forces proposed by Monaghan and Gingold (1983) to smooth out velocity oscillations.

$$\Pi_{AB} = \begin{cases} \frac{\alpha \cdot \bar{c}_{AB} \cdot \mu_{AB}}{\bar{\rho}_{AB}} & \text{if } v_{AB} \cdot r_{AB} < 0 \\ 0 & \text{if } v_{AB} \cdot r_{AB} > 0 \end{cases} \quad (3)$$

$$\mu_{AB} = \frac{h v_{AB} r_{AB}}{r_{AB}^2 + (0.1h)^2} \quad (4)$$

where $\alpha = 0.01$ and $\beta = 0$ are values for reproducing free-surface flows determined by Monaghan (2005), and h is the smoothing length that depends on the particle size d_x and the kernel function used. In this work, interpolation has been done using a Gaussian kernel, meaning that the smoothing length is three times the particle size. Generally, complex turbulence models require excessive computational cost. However, López *et al.* (2010) showed that Monaghan's artificial viscosity, defined by Eqs. (3) and (4), correctly reproduces viscous dissipation in flows with a Froude number lower than 5 without increasing too much the computational load.

Following the weakly compressible SPH method (W-SPH), the pressure field is calculated through an equation of state, Eq. (5), to relate pressure and density.

$$p_i = \frac{\rho_0 c_s^2}{\gamma} \left(\left(\frac{\rho_i}{\rho_0} \right)^{\frac{1}{\gamma}} - 1 \right) \quad (5)$$

where c_s is the speed of sound in the medium, ρ_0 is the reference density, and γ is a polytropic index which guarantees a rigid dependence between pressure and density. Monaghan (2005) suggested a value of 7 if water is to be simulated. In addition, following the indications from Monaghan (1992), c_s is ten times larger than the maximum flow velocity to ensure a fluid compressibility lower than 1%. This allows for the use of larger time steps satisfying the Courant condition.

2.2 Boundary Condition

The CFD literature includes a wide range of studies concerning developed methodologies to reproduce contour geometry in SPH. In his paper, Violeau and Rogers (2016) highlight three principal techniques: a) repulsive functions such as the Lennard-Jones Forces (Lennard-Jones (1924)), b) fictitious particles, also known as ghost particles (Randles and Libersky (1996)) and c) the boundary integrals method (Kulasegaram *et al.* (2004)). All these commonly used boundary methods are adequate to contain the fluid particles inside the contour geometry, but the roughness they generate cannot be associated to physical values of friction.

Due to its lower computational cost and its better adaptation to complex geometries (López *et al.* (2016)), the Lennard-Jones repulsive forces scheme has been selected in this research for the implementation of the new Boundary Friction Force formulation. Back in 1994, Monaghan (1994) proposed the use of this method where the boundary is composed of fixed particles that exert a force over the approaching fluid particles. When the distance between the fluid and the boundary

particles r , is lower than a radius of action r_0 , the boundary particle exercises a radial repulsive force against the fluid particle. The value of this force per unit mass is defined by Eq. (6).

$$f(\bar{r}) = d_0 \left(\left(\frac{r_0}{r} \right)^{p_1} - \left(\frac{r_0}{r} \right)^{p_2} \right) \frac{\bar{r}}{r^2} \quad (6)$$

It can be seen that this force becomes zero when r is larger than r_0 . The constant d_0 has dimensions of velocity squared and allows for the regulation of the force module. Rogers and Dalrymple (2005) expressed d_0 as a proportional value of $g \cdot H$, where H denotes water depth and g the gravitational acceleration. According to the investigation made by Lenard-Jones, values of $p_1 = 4$ and $p_2 = 2$ are adopted (Lennard-Jones (1924)). Finally, the authors experience has shown that taking r_0 equal to the particle size leads to accurate results.

2.3 Spherimental

The appearance of graphic cards GPU (Graphics Processing Unit) and its massive expansion of the computation capacities has revolutionized the supercomputing world during the last decade. Following this new line of action, the Spanish Center for Public Works Studies and Experimentation (CEDEX) is developing an SPH model called SPHERIMENTAL with FORTRAN CUDA computing architecture. This software is capable of carrying out computational fluid dynamics (CFD) simulations by employing graphical processing unit computation as proposed by Hérault *et al.* (2010) and Crespo *et al.* (2011). The result is a considerable reduction of the computation complexity, which always has been the main drawback of the Lagrangian models.

Currently used as a complementary tool to physical experimentation in hydraulic studies at the Hydraulic Laboratory of CEDEX, SPHERIMENTAL is a SPH code that solves 2D and 3D Navier-Stokes equations for a monophasic and weakly compressible flow. This allows Navier-Stokes equations, Eqs. (1) and (2), to be integrated using an explicit time scheme. Integrations are computed with a Taylor Vortex Green third order Runge-kutta numerical scheme.

3. BOUNDARY FRICTION FORCE METHOD

The Boundary Friction Force method proposed in this paper adds a complementary shear stress at the boundaries to reproduce roughness friction. The approach implements an acceleration, opposite to the velocity vector, to those fluid particles interacting with the boundaries. Regardless of the boundary condition technique used to materialize the boundaries (repulsive functions, ghost particles or boundary integrals) the novel approach ensures the adequate three-dimensional simulation of open channel flows using the SPH method.

3.1 Shear Stress and Particle Acceleration

The use of the new procedure requires a proper

interpretation of the shear stress formulation commonly used for turbulent flows. Generally, as shown in Eq. (7), the bottom shear stress or bed resistance is expressed as a function of the so-called shear velocity v_* , or the square of the depth-averaged velocity V and a dimensionless friction coefficient C_f .

$$\tau_b = \rho v_*^2 = \rho C_f V^2 \quad (7)$$

Both concepts, shear velocity v_* , and depth-averaged velocity V , are easily handled in Eulerian models. However, they cannot be transposed to Lagrangian models in which particles carry the fluid properties. This is why, instead of defining shear stress as written in Eq. (7), the velocity of the fluid particle that interacts with the boundary is used. Such velocity is denoted in this paper as v_{part} and it is responsible of the additional friction acceleration adopted for this new boundary method. Equation (8) provides a dimensionally correct expression for the shear stress:

$$\tau_{f,SPH} = \rho v_*^2 = \rho C_{rough} v_{part}^2 \quad (8)$$

Taking into account the force of flowing water acting on the bed and Newton's Second Law, the acceleration exerted by the boundary particles over the fluid particles yields:

$$a_f = \frac{C_{rough}}{d_x} v_{part}^2 \quad (9)$$

where C_{rough} is the proposed roughness coefficient, and d_x corresponds to the fluid particle size.

3.2 Free-Surface Uniform Steady Flow

The free-surface uniform steady flow has been subject of numerous investigations. Thus, its complete description considering the channel bed as the only source of friction is fully available in the scientific literature, providing a very appropriate framework for the calibration of the method. Since SPHERIMENTAL solves the Navier-Stokes equations in the $x - z$ plane, the results obtained in the case study test could be extrapolated to three-dimensional simulations by implementing the same boundary friction condition for the walls.

By definition, in uniform steady flows, the flow depth does not vary in time at every cross section, being, at the same time, constant along the flow direction. Because the acceleration is zero, flow depth and velocity remain constant throughout the entire channel length. Hence, the free surface slope S_w is equal to the bed slope S_0 , and the dynamic equilibrium equation then reduces to an algebraic equation of the equilibrium between the downslope component of the fluid weight and the boundary resistance:

$$S_w = \frac{\tau_b}{\rho g R_h} = \frac{\partial z}{\partial x} = S_0 \quad (10)$$

where S_w is the water surface slope, S_0 is the channel bottom slope, τ_b is the bottom shear stress, R_h is the hydraulic radius, and x and z are the

longitudinal and vertical spatial dimensions respectively. The friction slope can also be calculated using the widely used Manning's equation, Eq. (11):

$$S_w = \frac{n^2 V^2}{R_h^{4/3}} \quad (11)$$

Schlichting (1979), Nezu and Rodi (1986) and Garcia (2008) established that if the above-listed conditions are met, the velocity profile along the flow direction can be fitted to a logarithmic law, according to the equation:

$$\frac{v(z)}{v_*} = \frac{1}{k} \cdot \ln\left(\frac{z}{k_s}\right) + 8.5 \quad (12)$$

where $v(z)$ denotes the velocity at z distance from the channel bottom, k is a constant equal to 0.4 named after Von Karman, v_* is shear velocity and k_s is the roughness height defined by Nikuradse (Nikuradse (1933)). Integration of Eq. (12) over the depth yields the following expression for the depth-averaged velocity V :

$$V = \frac{v_*}{k} \cdot \ln\left(\frac{11R_h}{k_s}\right) \quad (13)$$

In steady, uniform flow, the forcing and the resistance are in balance. Using the dynamic equilibrium equation and assuming that $R_h \approx H$, the bed shear stress profile in a fully developed flow yields:

$$\tau(z) = \rho g (H - z) S_0 \quad (14)$$

Finally, Nikuradse's roughness height, k_s , can be related to the Manning's coefficient by Eq. (15):

$$k_s = 11 \cdot R_h \cdot e^{-\left(\frac{kR_h^{1/6}}{n \cdot g^{1/2}}\right)} \quad (15)$$

3.3 Roughness Coefficient

The formulation presented in Eq. (9) shows how the applied acceleration relates to the square of the particle velocity, the fluid particle size and the proposed roughness coefficient. Nonetheless, the equation does not give the proper insight into the distance at which this acceleration should be applied to obtain the same roughness effects as the observations or into how the friction condition can be fitted to a desired Manning's or Nikuradse's roughness value.

In the Eurlian turbulent flow theory, the friction coefficient depends on two dimensionless parameters, Eq. (16). The relative roughness which relates bottom roughness size k_s , to water depth H , and the Reynolds number, which associates viscous forces to inertia forces.

$$\tau_b = \rho V^2 \Psi\left(\frac{k_s}{H}, \frac{VH}{\nu}\right) \quad (16)$$

Following a similar approach, and in means of assuring the hydraulic similarity of the new formulation, the roughness coefficient C_{rough} also

depends on two dimensionless numbers, the dimensionless discretization number D_a , which is associated with geometrical dimensions similar to the relative roughness, and Monaghan's artificial viscosity parameter α .

$$C_{rough} = \Psi(D_a, \alpha) \quad (17)$$

López *et al.* (2016) pointed out that a proper fluid particles discretization is very important in order to obtain good results in numerical simulations. Once the steady-state regime condition is reached, H becomes constant and it is possible to check the discretization suitability by a dimensionless number, D_a :

$$D_a = \frac{d_x}{H} \quad (18)$$

Considering a steady-state regime, the velocity profile can be expressed as a function of two coefficients a and b :

$$v(z) = a \cdot \ln\left(\frac{z}{k_s}\right) + b \quad (19)$$

In general, when modeling a river reach, the flows of interest have high Reynolds numbers, so that viscous effects can be ignored, leaving the inertial effects as principal cause of the momentum transfer. As such, the bed shear stress for turbulent flows can also be expressed as:

$$\tau(z) = \rho \nu_t \frac{dv}{dz} \quad (20)$$

where ν_t refers to the kinematic turbulent viscosity. Considering Eqs. (19), (14) and (20), and assuming a hydraulic radius equal to the water depth, the kinematic turbulent viscosity presents a parabolic profile defined in the following equation, Eq. (21):

$$\nu_t(z) = \frac{gS_0}{a}(H - z) \cdot z \quad (21)$$

In steady-state flow with known discharge rate, q , and depth, H , the depth-averaged velocity can also be calculated. Thus, the b coefficient from Eq. (19) yields:

$$b = V - a \cdot \left(\ln\frac{R_h}{k_s} - 1\right) \quad (22)$$

Once the velocity profile has been obtained, the effective distance from boundary to resultant friction shear stress d_e , can be determined:

$$\begin{aligned} \tau(H - d_e) &= \rho g (H - d_e) S_0 = \rho C_{rough} \nu_{part}^2 = \\ &= \rho C_{rough} \left(a \cdot \ln\frac{d_e}{k_s} + b\right)^2 \end{aligned} \quad (23)$$

Figure 2 illustrates the mentioned effective distance d_e . Since the interest lies upon developing a formulation based on the discretization number and thus, the fluid particle size, a the dependence between d_e and the particle discretization size d_x , Eq. (24) has been proposed. The equation allows to

obtain the value of the effective distance, d_e , as a function of d_x by means of a coefficient C_e .

$$d_e = C_e \cdot d_x \quad (24)$$

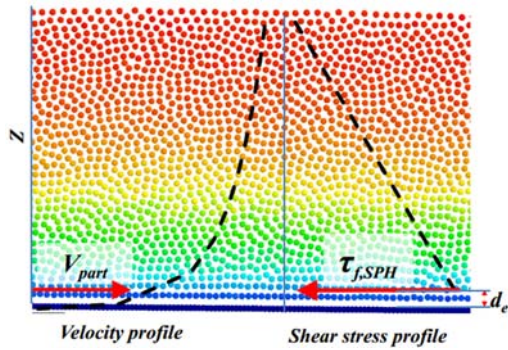


Fig. 2. Friction stress application distance.

Once the velocity and the turbulence profiles are known, it is possible to obtain the formulation that gives the roughness coefficient. This coefficient is assigned to contour particles to reproduce flow resistance associated with a given Nikuradse's k_s or Manning's n coefficients. From the shear stress equilibrium proposed in Eq. (23) and taking into account Eq. (11), a value for the new friction coefficient is obtained, Eq. (25).

$$C_{rough} = \frac{g(H - C_e d_x)}{H^{4/3}} n^2 \left(\frac{a \left(\ln \frac{H}{k_s} - 1 \right) + b}{a \left(\ln \frac{C_e d_x}{k_s} \right) + b} \right)^2 \quad (25)$$

4. OPEN CHANNEL FLOW CASE STUDY

The proposed methodology has been analyzed and calibrated by means of a very simple case study composed of a rectangular-shaped straight channel with uniform steady flow and considering the channel bed as only source of friction. In order to properly characterize that bottom friction, experiments have been designed in supercritical regime. As such, it is assured that downstream boundary conditions do not affect the water surface levels up-stream. The supercritical regime conditions have been achieved for all tested flow rates by adopting a 1% channel bed slope.

To produce useful outcomes for the comparison and calibration of the methodology with the theoretical values, an uniform steady flow must be guaranteed for all the simulations. With this regard, the simulations were kept running until the out-flow rates equalized the inflows to ensure a constant flow rate in the entire channel length. Furthermore, the cross section was maintained constant along the entire tested channel. Lastly, to comply with the uniform condition, the tested channel longitudes were accommodated for each test with the purpose

of reaching the equilibrium between water weight, viscous forces and bottom friction. Depending on the flow rate q , the upstream water depth H and the bottom friction n (or k_s), lengths varied from 400m up to 1500m.

Finally, the fluid particle size, d_x , and the distance between boundary particles, d_{xc} , have been set to 0.1m and 0.04m respectively for all the simulations. The motivation behind choosing d_{xc} to be slightly smaller than half of d_x lies in the fact that a uniform boundary force field and the prevention of fluid particles leakage must be guaranteed for the correct performance of the SPH model.

5. RESULTS AND DISCUSSIONS

In this section, the results obtained in the calibration tests using the described case study are presented. First, the flow resistance generated purely by the Lennard-Jones forces has been studied. Then, the influence the dimensionless discretization number D_a and the viscous parameter α have over the suggested roughness coefficient are analyzed. Lastly, and in accordance with the results obtained from those dependence studies, a similarity criterion based on Von Karman's constant is proposed.

5.1 Flow Resistance Due To Lennard-Jones Forces

The first tests have been carried out solely considering the Lennard-Jones forces, to quantify the resistance to the flow exerted by the commonly used boundary technique. The parameters from Eq. (6) have been taken as $d_0 = 10$, $p_1 = 4$, and $p_2 = 2$, with r_0 equal to fluid particles size, d_x .

Figure 3 shows the velocity and water depth profiles obtained when a unitary flow rate $q = 10m^3/s/m$ is simulated in the described channel. Despite the large channel length adopted, the flow presents a constant acceleration, reaching high velocities without achieving a steady-state regime. This implies that the boundary roughness is basically zero, which is not realistic for bottom friction in open channel flow. Consequently, it has been concluded that the boundary roughness reproduced by the Lennard-Jones repulsive forces is too weak to cause the adequate resistance to flow.

5.2 Roughness Coefficient Dependence Studies

As stated in Eq. (18), Crough depends on two dimensionless numbers, the discretization number D_a , and the artificial viscous parameter α . The developed tests have shown a clear impact of both parameters on the simulations results. This is the reason why their effect has been investigated.

In order to study the influence of fluid discretization D_a , forty five simulations have been conducted. Keeping Monaghan's artificial viscosity coefficient

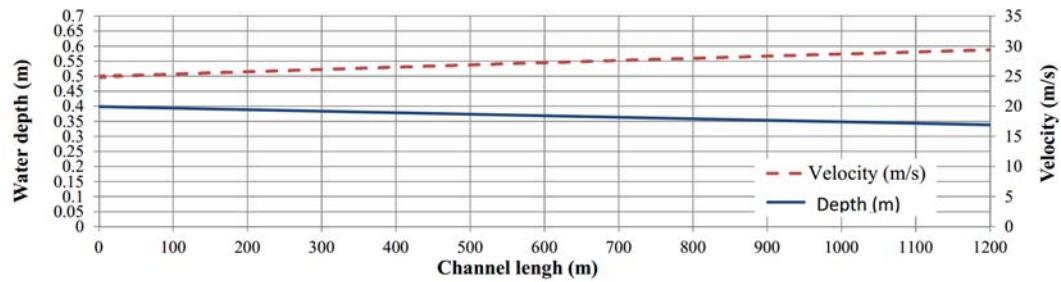


Fig. 3. Depth and velocity profile. $q = 10\text{m}^3/\text{sm}$.

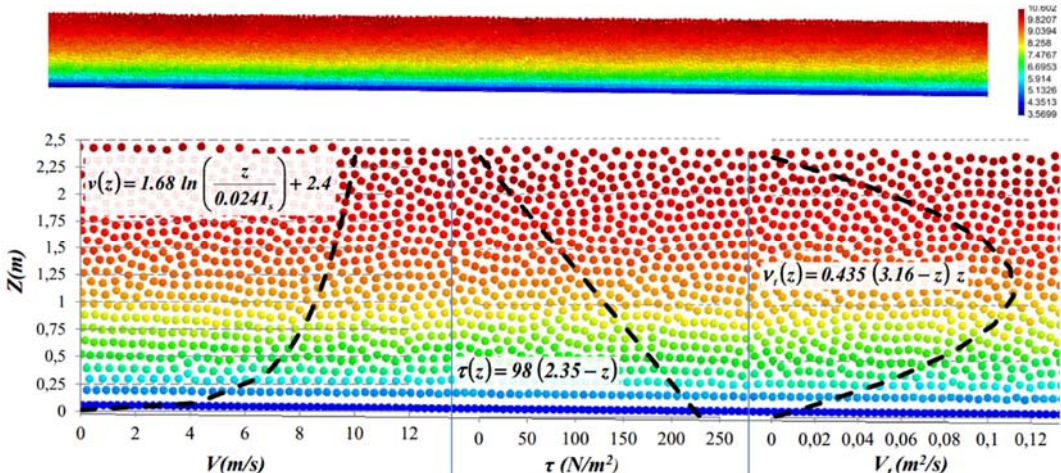
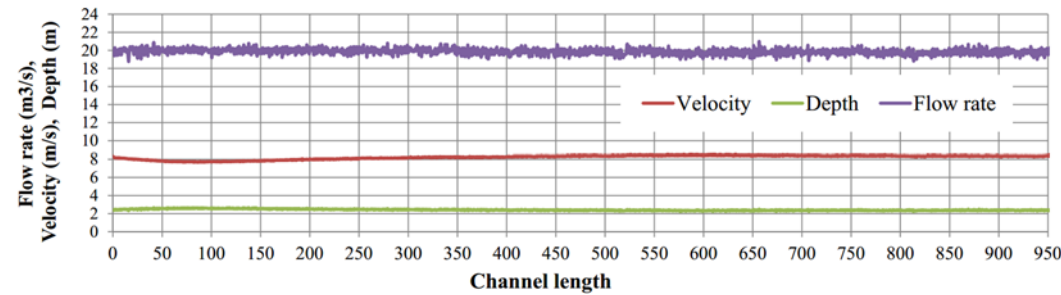
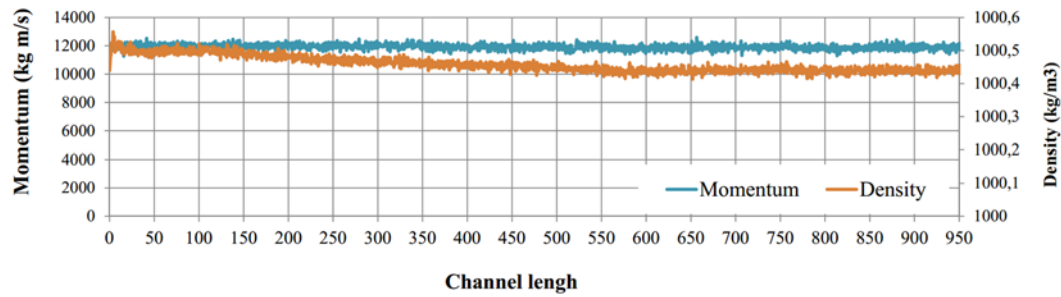


Fig. 4. Example test graphical results with flow rate $q = 20\text{m}^3/\text{s}/\text{m}$: channel length $L = 950\text{m}$: uniform steady depth $H = 2.35\text{m}$: Manning's roughness $n = 0.0212$.

constant and equal to $\alpha = 0.01$ in all tests, different roughness values, varying from 0.0005 to 0.01, have been applied. Each experiment required several repetitions in which the initial depth, the channel length and simulation time were modified until the steady-state flow regime was achieved. Out-comes from all the performed tests are summarized in Table 1.

Cross sections along the channel distributed each half a meter measured the mean velocity, flow rate, momentum, average density and velocity profiles of every test. Figure 4 displays the graphical results obtained from an example test with an unitary flow rate equal to $q = 20\text{m}^3/\text{s}/\text{m}$ and $C_{rough} = 0.008$. The velocity profile along the channel axis shows that at least a 600m channel was necessary to reach the

Table 1 Summary of the tests performed with the artificial viscosity parameter $\alpha = 0.01$

C_{rough}	q (m ² /s)	H (m)	Da	v^* (m/s)	n (m ^{1/6})	ks (mm)	a	b	C_e
0,0005	5	0,570	0,175	0,236	0,00779	0,00006	0,12	7,80	1,75
0,0005	10	0,860	0,116	0,290	0,00794	0,00007	0,31	8,70	2,17
0,0005	20	1,296	0,077	0,356	0,00778	0,00006	0,65	9,30	2,02
0,0005	40	1,943	0,051	0,436	0,00802	0,00007	0,85	9,00	4,83
0,0005	60	2,446	0,041	0,490	0,00791	0,00007	1,44	9,20	2,30
0,0005	80	2,958	0,034	0,538	0,00789	0,00006	1,81	9,30	1,60
0,001	2	0,401	0,250	0,198	0,01107	0,00049	0,11	4,30	1,61
0,001	5	0,697	0,143	0,261	0,01103	0,00048	0,23	5,65	1,92
0,001	10	1,030	0,097	0,318	0,01103	0,00048	0,40	6,60	2,05
0,001	20	1,577	0,063	0,393	0,0109	0,00045	0,83	6,40	2,16
0,001	40	2,324	0,043	0,477	0,0107	0,00040	1,29	6,50	1,89
0,001	60	2,859	0,035	0,529	0,01031	0,00032	1,95	3,80	1,83
0,001	80	3,327	0,030	0,571	0,01009	0,00028	1,85	6,25	1,35
0,001	120	4,133	0,024	0,636	0,0098	0,00024	3,07	-0,80	1,89
0,002	2	0,490	0,204	0,219	0,01547	0,00364	0,13	3,50	1,69
0,002	5	0,836	0,120	0,286	0,0151	0,00315	0,32	4,43	1,77
0,002	10	1,282	0,078	0,355	0,01513	0,00319	0,47	5,45	1,63
0,002	20	1,909	0,052	0,432	0,0148	0,00279	0,92	5,30	1,75
0,002	40	2,770	0,036	0,521	0,01382	0,00185	1,49	4,78	1,87
0,002	60	3,314	0,030	0,570	0,01286	0,00120	2,49	0,10	1,53
0,002	80	3,747	0,027	0,606	0,01261	0,00107	2,63	0,52	1,81
0,002	120	4,431	0,023	0,659	0,01187	0,00074	3,06	-1,08	1,65
0,003	1	0,363	0,276	0,188	0,0185	0,01066	0,09	2,53	1,30
0,003	2	0,548	0,182	0,232	0,01865	0,01119	0,17	3,10	1,63
0,003	5	0,935	0,107	0,303	0,01811	0,00938	0,40	3,82	1,76
0,003	10	1,392	0,072	0,369	0,01738	0,00733	0,74	3,97	1,74
0,004	1	0,392	0,255	0,196	0,0213	0,02482	0,08	2,35	0,28
0,004	2	0,593	0,169	0,241	0,0213	0,02482	0,17	2,95	1,58
0,004	5	0,999	0,100	0,313	0,0203	0,01860	0,47	3,60	1,49
0,004	10	1,468	0,068	0,379	0,0192	0,01332	0,84	3,60	1,56
0,004	20	2,172	0,046	0,461	0,01845	0,01048	1,24	3,70	1,45
0,004	40	3,137	0,032	0,554	0,0169	0,00619	2,04	2,30	1,37
0,004	120	6,131	0,016	0,775	0,01662	0,00560	3,95	-3,30 2,	2,69
0,006	1	0,447	0,224	0,209	0,0261	0,08403	0,10	2,15	1,48
0,006	5	1,103	0,091	0,329	0,02381	0,04843	0,50	3,45	1,38
0,006	10	1,578	0,063	0,393	0,02176	0,02822	1,00	3,25	1,40
0,006	20	2,330	0,043	0,478	0,0204	0,01916	1,74	2,00	1,83
0,006	40	3,319	0,030	0,570	0,0186	0,01101	2,25	1,50	1,40
0,006	120	6,348	0,016	0,789	0,0175	0,00764	3,97	-3,90	2,30
0,008	5	1,167	0,086	0,338	0,0261	0,08403	0,56	3,30	1,27
0,008	10	1,698	0,059	0,408	0,024	0,05080	1,20	2,90	1,65
0,008	20	2,354	0,042	0,480	0,0212	0,02413	1,68	2,40	1,29
0,01	5	1,219	0,082	0,346	0,028	0,12810	0,60	3,28	1,18
0,01	10	1,771	0,056	0,417	0,0257	0,07659	1,32	2,85	1,77
0,01	20	2,425	0,041	0,487	0,0221	0,03097	1,86	1,90	1,39

uniform steady flow. The flow rate graph certifies that the steady state flow has been achieved at the downstream channel sections with a stabilized uniform depth of $H = 2.35m$. Finally, the momentum along the channel axis and the section average density remain constant for the achieved steady regime.

The influence of the discretization degree can be appreciated in Fig. 5, where the values from Table 1 relating Manning's and Nikuradse's coefficients with the dimensionless discretization number D_a have been drawn. To facilitate the interpretation of

the graph, tests with same C_{rough} have been grouped by colors. In addition, curves for each C_{rough} value have been plotted, choosing C_e as the mean value of all simulations ($C_e = 1.74$). Good fit can be observed.

A more detailed analysis of the results from Table 1 shows a direct relation between the velocity profile obtained from SPH simulation, expressed in terms of the ratio a/v^* and the discretization number D_a (see Fig. 6). By fitting the experimental values to a potential function, the following mathematical relationship has been obtained:

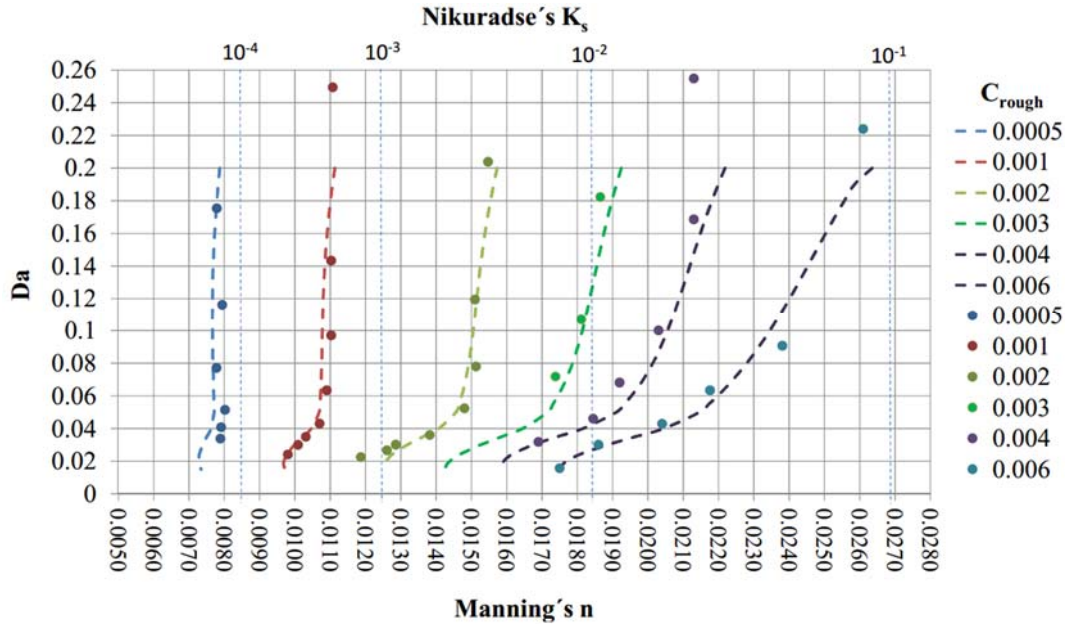


Fig. 5. C_{rough} curves relating Manning's n coefficient and D_a discretization dimensionless number.

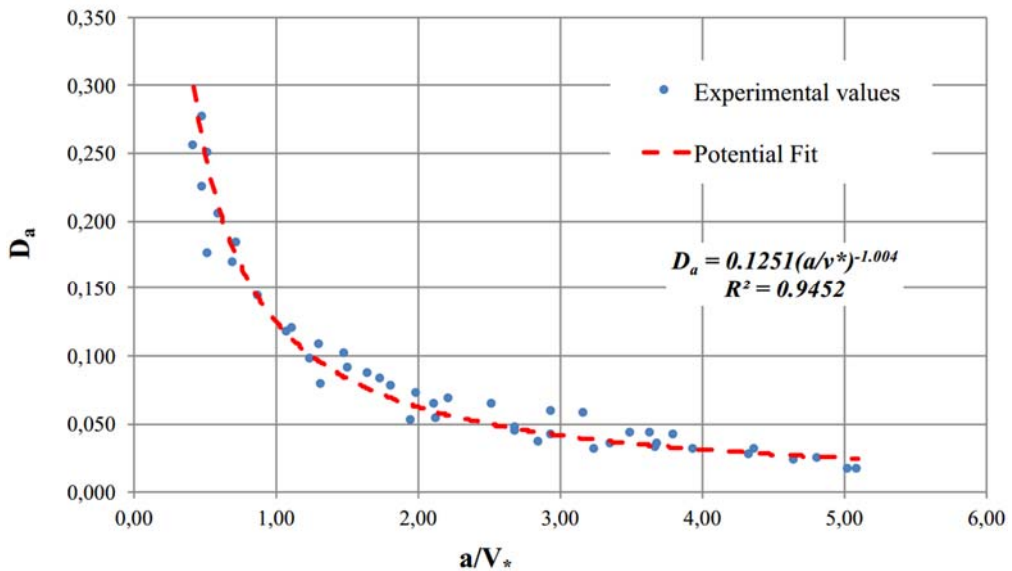


Fig. 6. Relationship between a and shear stress velocity v_* .

$$a = \frac{v_*}{8 \cdot D_a} \quad (26)$$

Taking into account this dependence, and comparing the coefficient a from Eq.(19) with the theoretical parameters from the free-surface uniform steady flow velocity profile, a relation between Von Karman's constant and the discretization has been discovered:

$$\frac{1}{k} = \frac{1}{8 \cdot D_a} \quad (27)$$

Since Von Karman's constant is equal to $k = 0.4$, a discretization number $D_a = 0.05$ makes true the previous equation. It is concluded that when an

artificial viscous parameter $\alpha = 0.01$ is used for simulating open channel flow with SPH, fluid particles sizes equal to $d_x = H \cdot 0.05$ guarantees the results representativeness.

However, as soon as the artificial viscosity value changes, Eq. (27) is no longer valid. For that reason, the dependence between C_{rough} and the viscosity has also been investigated. To do so, a new set of simulations with different α coefficients has been carried out. Results are summarized in Table 2 and plotted in Fig. 7a. By grouping the performed tests with the same α coefficient, it is possible to perform an analysis similar to the one already done for the first series of tests. For each test group the same adjustment depending on a C_a value, Eq. (28), has

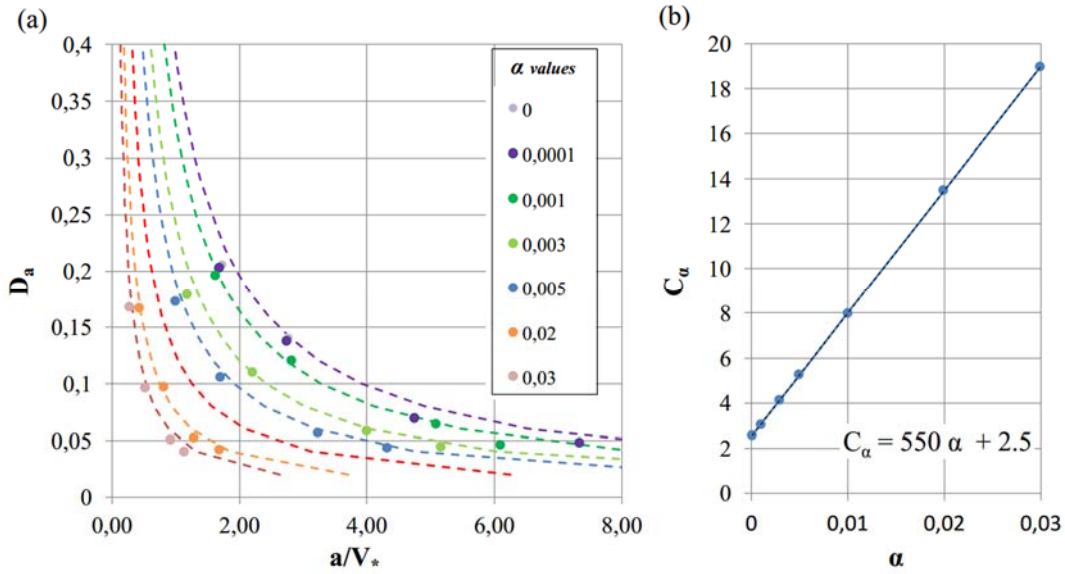


Fig. 7. Test with different viscosity coefficients α . a) Relationship between a/v_* and Da to each α values. b) Relationship between α and C_α .

Table 2 Summary of the tests done to analyze the influence of the artificial viscosity parameter α

α	C_{rough}	q (m ² /s)	H (m)	v^*	a	Da	a/v^*
0	0,002	20	1,460	0,378	1,800	0,068	4,759
0	0,004	5	0,715	0,265	0,734	0,140	2,774
0	0,004	2	0,487	0,219	0,378	0,205	1,730
0,0001	0,002	20	1,445	0,376	1,787	0,069	4,749
0,0001	0,004	5	0,726	0,267	0,734	0,138	2,752
0,0001	0,004	2	0,492	0,220	0,370	0,203	1,686
0,0001	0,001	40	2,095	0,453	3,329	0,048	7,348
0,001	0,002	20	1,571	0,392	1,994	0,064	5,082
0,001	0,004	5	0,835	0,286	0,809	0,120	2,826
0,001	0,004	2	0,510	0,223	0,365	0,196	1,631
0,001	0,001	40	2,183	0,463	2,821	0,046	6,098
0,003	0,002	20	1,718	0,410	1,644	0,058	4,007
0,003	0,004	5	0,910	0,299	0,659	0,110	2,205
0,003	0,004	2	0,560	0,234	0,277	0,179	1,181
0,003	0,001	40	2,282	0,473	2,442	0,044	5,163
0,005	0,002	20	1,763	0,416	1,345	0,057	3,235
0,005	0,004	5	0,946	0,304	0,519	0,106	1,705
0,005	0,004	2	0,579	0,238	0,239	0,173	1,005
0,005	0,001	40	2,293	0,474	2,046	0,044	4,316
0,02	0,002	20	1,912	0,433	0,556	0,052	1,285
0,02	0,004	5	1,035	0,318	0,261	0,097	0,818
0,02	0,004	2	0,600	0,243	0,107	0,167	0,439
0,02	0,001	40	2,397	0,485	0,822	0,042	1,696
0,03	0,002	20	1,981	0,441	0,404	0,050	0,916
0,03	0,004	5	1,045	0,320	0,166	0,096	0,517
0,03	0,004	2	0,596	0,242	0,069	0,168	0,286
0,03	0,001	40	2,506	0,496	0,564	0,040	1,138

been found. Hence, it can be seen that Eq. (28) is a generalization of Eq. (26) for different viscosity values.

$$a = \frac{v_*}{C_\alpha Da} \quad (28)$$

Figure 7b shows the dependency between a and α through the coefficient C_α . The obtained lineal adjustment for such parameter is presented in Eq. (29).

$$C_\alpha = 550\alpha + 2.5 \quad (29)$$

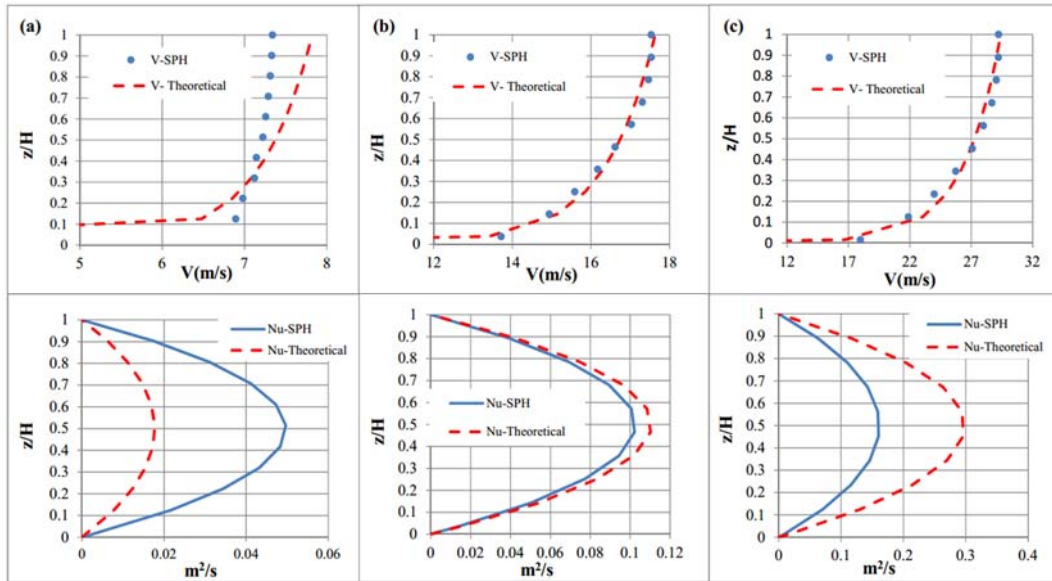


Fig. 8. a) $C_a D_a = 1.17$. $C_{rough} = 0.001$; $q = 5m^3/s$; $H = 0.70m$; $n = 0.01103m^{1/6}$; b) $C_a D_a = 0.35$. $C_{rough} = 0.001$; $q = 40m^3/s$; $H = 2.32m$; $n = 0.0107m^{1/6}$; c) $C_a D_a = 0.18$. $C_{rough} = 0.001$; $q = 120m^3/s$; $H = 4.13m$; $n = 0.0098m^{1/6}$.

5.3 Similarity Criterion

According to the simulations results shown in Table 1 and Table 2, and the expressions obtained from the dependence analysis, a new similarity criterion has been developed. Following the relation suggested in Eq. (28), it yields that the Von Karman’s constant must be equal to the product between C_a and D_a as shown in Eq. (30):

$$\frac{C_a D_a}{k} = 1 \quad (30)$$

Figure 8 shows the importance of selecting an adequate particle size or artificial viscosity parameter. When the proposed similarity criterion is met, the accordance between the velocity profile obtained with the SPH numerical simulation and the logarithmic velocity profile that results from the theory of turbulent boundary layer flow (Eq. (12)) is guaranteed.

On the one hand, if $C_a \cdot D_a > k$, SPH model simulations become excessively turbulent. It can be seen in Fig. 8a how the velocity profile homogenizes faster than the theoretical profile for high values of D_a numbers (or low discretization of the continuum). On the other hand, when $C_a \cdot D_a \approx k$, both the results from the SPH model velocity profile and the kinematic turbulent viscosity law agreed with the theoretical ones (Fig. 8b). By selecting a lower coefficient of viscosity α , a large D_a number is required to maintain this proportionality. Thus, the relative size of SPH particles increases. This means that by using low α values, an open channel flow case is correctly reproduced with a lower computational cost. However, it should also be noted that the stability introduced by the viscous term is lost when low coefficients are used. Finally, if $C_a \cdot D_a < k$, SPH simulations not only provide lower viscosity

than the theoretical parabolic model but also velocity profiles that are smoother than the profiles suggested by the theoretical knowledge (Fig. 8c).

The relationship pointed out in Eq. (30) allows the presetting the SPH model. If the flow rate and the approximate water depth are known, it is possible to determine the fluid particle size and the viscosity coefficient to be used in SPH simulation. This is extremely important for optimizing these simulations. In order to clarify the resolution process according to the recommended similarity criterion, the flow chart displayed in Fig. 9 is presented.

6. CONCLUSIONS

Up to this day, the lack of a boundary methodology capable of correctly recreating boundary roughness effects has hindered the use of the SPH method to simulate three-dimensional open channel flow scenarios, in which the water surface is largely influenced by the boundary friction. As part of this investigation, it was demonstrated how the boundary roughness reproduced by one of the most widely used boundary techniques, the Lennard-Jones repulsive forces, is too weak to offer an adequate resistance to flow.

In this paper, the authors have presented an original formulation to reproduce flow resistance in open channel flow using SPH. The Boundary Friction Force method implements contour shear stress by adding an extra acceleration to the fluid particles interacting with the boundaries. Furthermore, the suggested roughness coefficient C_{rough} allows to fit the friction condition to a desired Manning’s n or Nikuradse’s k_s roughness value, increasing the applicability of the approach.

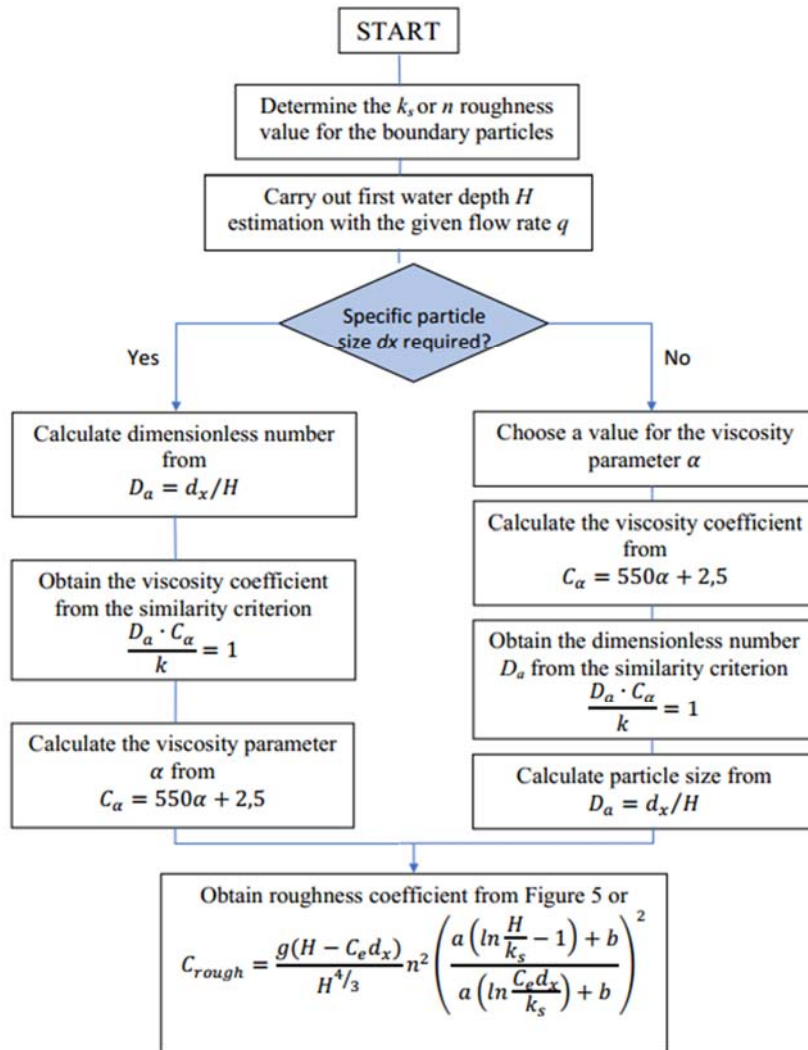


Fig. 9. C_{rough} calculation flow chart in accordance with the similarity criterion.

The proposed method has been tested and calibrated by means of a very simple case study composed of a rectangular-shaped straight channel with uniform steady flow. Although the formulation can be adapted to any of the current boundary methodologies used to materialize the boundaries, only the Lennard-Jones repulsive forces scheme has been selected in this research due to its lower computational cost and its better adaptation to complex geometries. Future investigations could be dealing with the implementation of the method to those remaining boundary techniques.

Finally, the presented work offers a general formulation for the velocity and turbulent viscosity profiles that will be obtained in a three-dimensional SPH simulations as a function of two dimensionless parameters: the relative particle size, D_a , and the artificial viscosity coefficient, α . The influence those parameters have on the results of the simulations has been analyzed, leading to the formulation

of a novel hydraulic similarity criterion which guarantees representativeness of SPH simulations in

open channel flow.

To sum up, this research gives solution to two of the main drawbacks of using the SPH method to reproduce three-dimensional OCF scenarios. First, introduces a new boundary friction condition that enables the adequate simulation of roughness effects, and second, proposes a similarity criterion which helps reducing the computational load and guarantees the simulation representativeness.

ACKNOWLEDGMENTS

We would like to thank CEDEX for supporting this research, especially to Jose María Grassa, CEDEX SPH pioneer.

REFERENCES

Chen, R., S. Shao, X. Liu, and X. Zhou (2015). Applications of Shallow Water SPH Model in Mountainous Rivers. *Journal of Applied Fluid Mechanics* 8(4), 863–870.

- Crespo, A. C., J. M. Dominguez, A. Barreiro, M. Gómez-Gesteira, and B. D. Rogers (2011). GPUs, a New Tool of Acceleration in CFD: Efficiency and Reliability on Smoothed Particle Hydrodynamics Methods. *PLOS ONE* 6(6), 1–13.
- García, M. H. (2008). *Sedimentation engineering: processes, measurements, modeling, and practice*. Reston, Va. : American Society of Civil Engineers.
- Gatti, D., A. Maffio, D. Zuccalá, and A. D. Monaco (2007). SPH simulation of hydrodynamics problems related to dam safety. In *Proc. 32nd Congress of the IAHR (CD-ROM)*, Number 2, Venice, Italy. IAHR.
- Gingold, R. A. and J. J. Monaghan (1977). Smoothed Particle Hydrodynamics - Theory and application to non-spherical stars. *Monthly Notices of the Royal Astronomical Society* 181, 375–389.
- Gómez-Gesteira, M., B. Rogers, R. Dalrymple, and A. Crespo (2010). State-of-the-art of classical SPH for free-surface flow. *Journal of Hydraulic Research* 48, 6–27.
- Grassa, J. (2007). Wave forces on a wavemaker. SPH simulation and comparison with analytic results. In *Proc. 32nd Congress of the IAHR*, Volume 1, Venice, Italy, pp. p. 100. IAHR.
- Héroult, A., G. Bilotta, and R. A. Dalrymple (2010). SPH on GPU with CUDA. *Journal of Hydraulic Research* 48(1), 74–79.
- Kazemi, E., A. Nichols, S. Tait, and S. Shao (2017). SPH modelling of depth-limited turbulent open channel flows over rough boundaries. *International Journal for Numerical Methods in Fluids* 83(1), 3–27.
- Kulasegaram, S., J. Bonet, R. W. Lewis, and M. Profit (2004). A variational formulation based contact algorithm for rigid boundaries in two-dimensional SPH applications. *Computational Mechanics* 33(4), 316–325.
- Lennard-Jones, J. (1924). On the determination of molecular fields from the equation of state of a gas. *Proceedings of the Royal Society of London A: Mathematical, Physical and Engineering Sciences* 106(738), 463–477.
- López, D. and V. Cuellar (2011). Paralelización CUDA del método SPH. Aplicaciones en el diseño de estructuras hidráulicas. In *Proc. III Jornadas de Ingeniería del Agua*, Barcelona. JIA.
- López, D., M. de Blas, R. Marivela, J. Rebollo, R. Díaz, M. Sánchez-Juny, and S. Estrella (2011). Estudio hidrodinámico de vertederos y rápidas escalonadas con modelo numérico tridimensional SPH: Proyecto ALIVESCA. In *Proc. II Jornadas de Ingeniería del Agua*.
- López, D., R. Díaz, J. Rebollo, T. Ramos, F. Andrés, and M. Berga (2016). Aplicación del método SPH al estudio hidráulico de estructuras. Análisis hidrodinámico del aliviadero en pozo de la presa de Nagore (Navarra). *RIBAGUA - Revista Iberoamericana del Agua* 3(1), 1 – 7.
- López, D., R. Marivela, and F. Aranda (2009). Calibration of SPH model using prototype pressure data from the stilling basin of the Villar del Rey dam, Spain. In *Proc. 33rd Congress of the IAHR*, Volume Water Engineering for a Sustainable Environment, Vancouver, pp. 9–14. IAHR.
- López, D., R. Marivela, and L. Garrote (2010). Smoothed particle hydrodynamics model applied to hydraulic structures: a hydraulic jump test case. *Journal of Hydraulic Research* 48(1), 142–158.
- Lucy, L. (1977). A numerical approach to the testing of the fission hypothesis. *Astronomical Journal* 82, 1013–1024.
- Lui, G. and M. Liu (2003). *Smoothed Particle Hydrodynamics. A meshfree particle method*, pp. 365–421. Singapore: WORLD SCIENTIFIC.
- Monaghan, J. (1994). Simulating Free Surface Flows with SPH. *Journal of Computational Physics* 110(2), 399 – 406.
- Monaghan, J. and R. Gingold (1983). Shock simulation by the particle method SPH. *Journal of Computational Physics* 52(2), 374 – 389.
- Monaghan, J. J. (1992). Smoothed Particle Hydrodynamics. *Annual Review of Astronomy and Astrophysics* 30(1), 543–574.
- Monaghan, J. J. (2005). Smoothed Particle Hydrodynamics. *Reports on Progress in Physics* 68(8), 1703.
- Nezu, I. and W. Rodi (1986). Openchannel Flow Measurements with a Laser Doppler Anemometer. *Journal of Hydraulic Engineering* 112(5), 335–355.
- Nikuradse, J. (1933). Stromungsgesetz in rauhren Rohren. *VDI Forschungsheft*, 361.
- Randles, P. and L. Libersky (1996). Smoothed Particle Hydrodynamics: Some recent improvements and applications. *Computer Methods in Applied Mechanics and Engineering* 139(1), 375 – 408.
- Rogers, B. and R. Dalrymple (2005, September 2004). SPH Modeling of breaking waves. In *Coastal Engineering 2004 - Proceedings of the 29th International Conference*, Lisbon, Portugal, pp. 415–427.
- Schlichting, H. (1979). *Boundary Layer Theory* (7th ed.). New York: McGraw-Hill.
- Violeau, D. and B. D. Rogers (2016). Smoothed particle hydrodynamics (SPH) for freesurface flows: past, present and future. *Journal of Hydraulic Research* 54(1), 1–26

